AIAA JOURNAL
Vol. 37, No. 2, February 1999

# Molecular Dynamics Simulation of Piston-Driven Shock Wave in Hard Sphere Gas

MyeungJouh Woo*
*NASA Lewis Research Center, Cleveland, Ohio 44135*
and
Isaac Greber†
*Case Western Reserve University, Cleveland, Ohio 44106*

**Molecular dynamics simulation is used to study the piston-driven shock wave at Mach numbers 1.5, 3, and 10. A shock tube, whose shape is a circular cylinder, is filled with hard sphere molecules having a Maxwellian thermal velocity distribution and zero mean velocity. The piston moves, and a shock wave is generated. The work is intended as an important test case of the application of molecular dynamics in fluid mechanical problems in a manner that avoids imposing statistical boundary conditions. Therefore, all collisions are treated as elastic, including those between the molecules and the computational boundaries, so that the shock development is entirely causal. The propagation and structure of the shock is examined in detail, and the wave speed; profiles of density, velocity, and temperature; and shock thickness are determined. The results are compared with published results of other methods, especially the direct simulation Monte Carlo (DSMC) method. Property profiles are similar to those generated by DSMC. Shock thicknesses are smaller than DSMC results but larger than those of the other methods.**

## Nomenclature

| | |
|---|---|
| $a$ | = speed of sound |
| $c$ | = thermal component of velocity |
| $c_{mp}$ | = most probable speed |
| $D$ | = diameter of the computational region |
| $d$ | = diameter of a particle |
| $E$ | = thermal energy |
| $Kn$ | = Knudsen number, $\lambda/D$ |
| $k$ | = Boltzmann constant |
| $L$ | = length of the computational region |
| $M$ | = Mach number |
| $m$ | = mass of a particle |
| $N$ | = total number of particles in the simulation |
| $n$ | = number density |
| $n_{qk}$ | = number density in the $q$th cell during the $k$th interval |
| $p$ | = pressure |
| $s$ | = mean center-to-center distance between particles |
| $s/d$ | = spacing ratio |
| $T$ | = temperature |
| $t$ | = time |
| $\bar{t}$ | = nondimensional time, $t/(\lambda/c_{mp})$ |
| $u, v, w$ | = velocity components in $x, y, z$ directions, respectively |
| $x, y, z$ | = Cartesian coordinates |
| $\gamma$ | = specific heat ratio, $\frac{5}{3}$ for hard sphere molecules |
| $\Delta$ | = shock thickness from the maximum slope definition |
| $\delta t_i$ | = time occupancy of the $i$th particle |
| $\lambda$ | = mean free path |
| $\mu$ | = viscosity coefficient |
| $\rho$ | = density |
| $\tau$ | = total time |

*Subscripts*

| | |
|---|---|
| $m$ | = measured |
| $p$ | = piston |
| $r$ | = reference |
| $s$ | = shock |
| 1 | = low-pressure region |
| 2 | = high-pressure region |

Received March 16, 1998; revision received Oct. 8, 1998; accepted for publication Oct. 14, 1998. Copyright © 1998 by the American Institute of Aeronautics and Astronautics, Inc. All rights reserved.

*National Research Council Fellow, Photo-Voltaic and Space Environment Effects Branch; currently Senior Mechanical Engineer, Osborn Engineering Company, 1300 East Ninth Street, Suite 1500, Cleveland, OH 44114.

†Professor, Department of Mechanical and Aerospace Engineering. Associate Fellow AIAA.

## I. Introduction

THE calculation of the structure of a shock wave is an old, traditional problem that has played an important role in the development of fluid mechanics and in the development of kinetic theory computations. Early investigations used the Navier–Stokes equation with constant coefficients of heat conduction and viscosity. These included the works of Rankine,[1] Lord Rayleigh,[2] and Taylor.[3] Rankine's work gave a solution for shock thickness considering heat conduction but not viscosity, whereas Taylor's solution considered viscosity but not heat conduction. Taylor also gave an explicit formula for weak shocks, which included the effects of both viscosity and heat conduction. Essential results of these early works are that the shock thickness decreases with increasing Mach number and that the thickness is of the order of a mean free path in the region upstream of the shock. More refined solutions of the Navier–Stokes equations were obtained by Becker[4] and by Thomas[5] but only for shocks below Mach number 2. A proof of the existence and uniqueness of the solution for a steady one-dimensional flow with small viscosity and heat conductivity was given by Gilbarg.[6] Von Mises[7] gave a simple method of estimating the upper and lower bounds of the shock thickness in a perfect gas. Departing from the Navier–Stokes equation, Zoller[8] obtained a solution to the Burnett equations, and early kinetic theory estimates included the Chapman–Enskog–Burnett iteration method[9] and the Grad[10,11] 13-moment method. All of the works just cited were for weak shocks. The Mott-Smith[12] bimodal model, which treats the distribution function in the shock region as a linear combination of the distribution functions for the upstream and downstream gases added to satisfy low-order moments of the Boltzmann equation, was probably the first kinetic theory approach to enable computations for strong shocks. A thoroughgoing reworking of the Navier–Stokes approach was done by Gilbarg and Paolucci,[13] and extensions of the Mott-Smith approach were given by Radin and Mintzer,[14] who used the bimodal distribution to generate an orthogonal polynomial expansion solution, and by Rode and Tanenbaum,[15] who generalized the computation by examining the effect of satisfying a higher-order moment rather than one of the lower-order moments. An entirely different kinetic theory approach

was initiated by Bird[16,17] with his direct simulation Monte Carlo method (DSMC); these computations not only provided shock profiles but also enabled the energy contributions of axial and lateral motions to be determined separately, showing the existence of a peak in axial temperature within the shock wave for strong shocks. Molecular dynamics (MD) has been used to obtain shock structure in liquids and in solids, for example, by Tsai and Trevino[18] and by Hoover,[19] but it appears that the only previous attempt to study the shock structure in a gas using MD was the exploratory work of Niki and Ono,[20] using only 135 hard sphere particles and achieving limited results.

The present work was designed to generate shock structure using MD, in a manner that avoids statistical boundary conditions. It is intended as an important test case of the application of MD in fluid mechanical problems. It was especially intended to perform the computations using boundary conditions that do not impose any features of the flow other than the main shock-wave-generating mechanism. Therefore, these computations were performed using only elastic collisions, including molecular collisions with boundaries, and, consequently, with no imposed dissipative mechanisms. For the purpose of avoiding statistical boundary conditions, an unsteady problem is formulated, the shock wave generated by a piston moving into a gas with an initially zero mean velocity. A similar computation, using DSMC, was made by Bird,[21] presenting contours of properties. As compared with the stationary shock problem, the moving shock problem allows cleaner boundary conditions, but the extraction of information from the raw computational data is more complicated.

The computations were performed as a part of the doctoral dissertation of Woo.[22] Portions of this work were presented previously,[23] along with a computer movie made from the results; stills from the movie have been published elsewhere.[24]

## II. Computational Method

The basic model and coordinate system are shown in Fig. 1. A set of spheres of equal diameter is located randomly within a circular tube. One desires a small number of spheres to keep down computational time and storage but a large number for a high-quality simulation. One tends to expect that an inordinately large number of particles might be needed to perform computations that provide satisfactory results for a gas. Fortunately, this is not so. Greber and Wachman[25] have shown that remarkably small numbers of particles are sufficient and that one can estimate the particle density in the simulation that is needed to achieve desired levels of agreement with gas behavior. The basic idea is that if the ratio of the distance between particle centers to the diameter of particles is sufficiently large then this ratio is no longer an important scaling parameter and that the Knudsen number, the ratio of mean free path to a characteristic length, becomes the sufficient gas length parameter to achieve approximate dynamic similarity. The spacing ratio then does not have to mimic the gas spacing ratio but merely be sufficiently large so that increases in spacing ratio do not significantly affect the nondimensional results. As for the geometry, the tube must be long enough, in units of mean free path, for full shock development and adequate data collection, and the tube diameter must be large enough so that the results do not depend on that diameter. The choices made are different at the several Mach numbers. To understand the geometric selection, first observe that the Maxwell mean free path is given by

$$\lambda = \frac{1}{\pi\sqrt{2}nd^2} \tag{1}$$

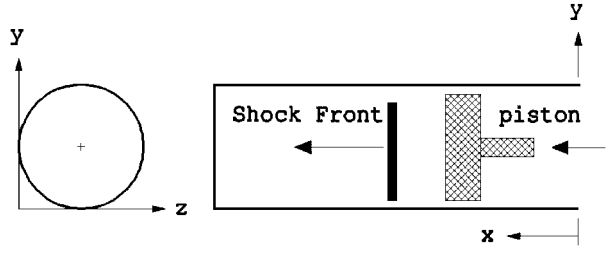


**Fig. 1 Piston-driven shock wave and coordinate system.**

**Table 1 Geometric parameters of computation**

| $M$ | $s_0/d$ | $d/\lambda_0$ | $\lambda_0/D$ | $L/\lambda_0$ | $N$ |
|---|---|---|---|---|---|
| 1.5 | 3.59 | 0.096 | 0.56 | 54 | 3000 |
| 3 | 4.33 | 0.055 | 0.81 | 49 | 4000 |
| 10 | 4.72 | 0.042 | 0.97 | 41 | 4000 |

From this, for a given number of particles $N$ and a given tube length $L$, the tube-to-particle diameter ratio is given by

$$\frac{D}{d} = \left[\frac{4\sqrt{2}N}{L/\lambda_1}\right]^{\frac{1}{2}} \tag{2}$$

The ratio of the tube diameter to the mean free path is given by

$$\frac{D}{\lambda} = 2^{\frac{7}{4}}\pi\sqrt{\frac{N}{L/\lambda_1}}\left(\frac{s}{d}\right)^3 \tag{3}$$

In Eqs. (2) and (3) the subscript 1 denotes conditions in the undisturbed gas, and the unsubscripted $s$ and $\lambda$ can refer to either the undisturbed or compressed gas. If the length ratio $L/\lambda_1$, the compressed gas spacing ratio $s_2/d$, and the number of particles $N$ are fixed, then the Knudsen number of the compressed gas, $\lambda_2/D$, is determined independently of the Mach number of the shock. However, the Knudsen number of the undisturbed gas, $\lambda_1/D$, then increases with increasing Mach number because of the decreasing ratio of upstream to downstream density across the shock wave. Correspondingly, the tube aspect ratio $L/D$ would increase with increasing Mach number. In the current work $s_2/d$ was held fixed at a value of 3; the remaining choices and geometric consequences are shown in Table 1. The selections were such that the Knudsen number of the undisturbed gas was never greater than unity.

The spheres are given initial velocities such that each Cartesian component of velocity is selected randomly within a Maxwellian distribution of velocities. For the purpose of this selection, the Maxwellian distribution is cut off at $\pm 3$ times the most probable speed. This cutoff captures 0.99998 of the integrated Maxwellian distribution.

The piston starts moving at the beginning of the simulation and continues to move at constant speed. A natural piston speed parameter would be the ratio of the piston speed to the most probable speed of the Maxwellian distribution of the undisturbed gas. Here, however, piston speeds were selected to correspond to theoretical shock Mach numbers of 1.5, 3, and 10, for the purpose of comparing the current results with published results using other methods. Using the shock jump relations in terms of the pressure ratio across the shock, the relationship between the shock Mach number and the piston Mach number, where each Mach number is defined as the ratio of the speed to the sonic speed of the undisturbed gas, is given parametrically by

$$\frac{M_2}{M_1} = \frac{2}{\gamma-1}\left(\frac{p_2}{p_1}-1\right)\Big/\left(1+\frac{\gamma+1}{\gamma-1}\frac{p_2}{p_1}\right) \tag{4}$$

$$\frac{p_2}{p_1} = 1+\frac{2\gamma}{\gamma+1}\left(M_1^2-1\right) \tag{5}$$

where $\gamma$ is the specific heat ratio (5/3 for monatomic gases) and $p_1$ and $p_2$ are the pressures on the low- and high-pressure sides of the shock wave, respectively. The speed of sound is related to the most probable speed by

$$a = \sqrt{\gamma/2}\,c_{\mathrm{mp}} \tag{6}$$

Consequently, the piston speed ratio is related to the shock Mach number by

$$\frac{u_p}{c_{\mathrm{mp}}} = \frac{(2\gamma)^{\frac{1}{2}}\left(M_1^2-1\right)}{(\gamma+1)M_1} \tag{7}$$

The particles are taken as rigid elastic spheres. Consequently, the particles move in straight lines at constant speed between instantaneous collisions. Collision occurs when the distance between

particle centers is the sum of the particle radii. This yields a quadratic equation in time for particle–particle collisions and a linear equation for particle–boundary collisions. The time to collide is computed for each pair, which can be a pair of particles or a particle and a boundary. A row-by-row search is made to find the first collision among all possible collision pairs. The outcome of that collision is determined by the dynamics of elastic collisions. The time to collide is then updated for any pair that has the current colliding pair as its member.

All collisions are taken as elastic, both particle–particle and particle–boundary. Only binary collisions are allowed. The simulation treats a simultaneous collision of three or more particles as sequential binary collisions. The outcome of a multiparticle interaction, in general, will be different from the sequential binary collision treatment; it is anticipated, however, that the multiparticle interaction is a rare event.

## III. Postprocessing of Data

The simulation described moves forward in time collision by collision rather than by specific time increments. After each collision the new velocities of particles that have just collided are written to an output file, which is then used to extract spatial and other information after the simulation is completed. Although the data sets generated are large, this separation of the dynamical process from the extraction of information has the advantage of being much faster than simultaneous processing, in our experience by about a factor of four. In addition, it allows the computation to be continued at a later date or for additional information to be extracted. The most time-consuming feature of the computational process is the computation of a new time to collide after each collision. For a system of $N$ particles this requires the solution of $N(N-1)/2$ quadratic equations for the particle-to-particle collisions, $2N$ linear equations for the particle-to-two-end-wall collisions, and $N$ quadratic equations for the particle-to-lateral-boundary collisions. However, we do not need to recompute the time to collide for particle pairs other than those involving one of the participants in the current collision. This reduces the time-to-collide computations to $2(N-2)$ quadratic equations for the particle-to-particle collisions plus 4 linear equations plus 2 quadratic equations for the boundary collisions. Clearly, only half this number of computations is needed after a collision with a boundary because only one particle is involved in the collision.

For the purpose of data collection, the computational region is divided into cells of equal width, which lie perpendicularly to the tube axis. The multiplicity of cells is roughly analogous to multiple measuring stations in a shock tube experiment. The location of a sphere is regarded as the location of its center. The center cannot be located closer than one radius from the contacting boundary; the region that can be occupied by particle centers defines the computational volume. The width of the cells is selected as one upstream mean free path. This size is selected primarily to allow direct comparison with DSMC results, obtained at corresponding resolution. This is also a reasonable choice; although a smaller width would yield apparently higher resolution, gas and flow properties change in spatial distances of the order of a mean free path, and so the increased computing requirements associated with smaller cells may not yield significantly improved results.

In principle, information from any single cell can be used to deduce shock profiles, as is done in a shock tube experiment with a single measuring station. Here, however, short-time-average values, i.e., time taken for the piston to move the distance of one mean free path, taken simultaneously over all of the cells, are used to represent instantaneous values and to provide a snapshot of the distribution of density and other properties. Values from the several cells are also combined to form composite profiles, providing a richer data set for final profiles.

Consider the density. The time-average density is defined as the total time of occupancy of particles in the region divided by the time of observation and the volume of the region. For a cell $q$ and a time interval $\tau$ at a time $t_k$, this instantaneous number density is given by

$$n_{q_k} = \frac{1}{N\ (\text{volume})}\left(\frac{\sum_i \delta t_i}{\tau}\right)_{q_k} \tag{8}$$

where $\delta t_i$ is the time interval that a particle $i$ spends in the cell during the period $\tau$. When these averages are performed over a set of values $t_k$, the result is an array describing the density as a function of longitudinal location $x$ and time. This array allows the construction of constant density contours in a space–time plot. This is done with the aid of a standard interpolation scheme, commercially implemented.[26] In this scheme a value of density at point $x, t$ is estimated, and the procedure finds values of the number density at a set of nearest neighbors to the selected point, which are found in a search procedure. The value finally chosen is a weighted average of the values at the neighbors, weighted in proportion to the inverse of the square of the distance in $x, t$ space from the selected location.

From these constant density profiles, which will be discussed in detail later, one observes that the shock wave travels at a constant speed, close to the theoretical continuum value. This feature is used to form composite $n$-vs-$x$ profiles from the instantaneous values. The profiles at all times can be shifted to a common $x$ location using the Galilean transformation

$$x = x_m - u_s(t_m - t_r) \tag{9}$$

where $x$ is the effective location, $x_m$ and $t_m$ are the measured values, $u_s$ is the shock speed, and $t_r$ is the common reference time, for example, the time of the first snapshot. After the shift, the $x$ values are relocated to the centers of the bins at the shifted locations.

Corresponding snapshot values and composite profiles are obtained for the mean velocity components and the kinetic energy of thermal motion, which yields the temperature. For any $k$th set, the mean velocity is defined as the sum of velocities divided by the number of particles observed in the region during an interval of time:

$$u = \frac{1}{N}\sum_{i=1}^{N} u_i \tag{10}$$

The thermal energy is the kinetic energy associated with the deviation of the velocity from the mean value. This is given by

$$E = (1/2)m\langle c^2\rangle = (3/2)kT \tag{11}$$

## IV. Computational Errors

Final runs were performed using the Cray YMP C90 at the NASA Ames Research Center. The execution speed was $160 \times 10^6$ floating-point operations per second, without any special effort to vectorize the source code. A typical run using 4000 particles and 100,000 interactions required about 4 CPU hours to complete the dynamics portion of the simulation, then about 400 CPU seconds to analyze the output files to produce final results.

Error in coordinates of the particle centers is the first concern. The repeated process of updating the location of particles can propagate errors in location. This is an extremely significant problem because the algorithm uses the locations to compute collision times. The existence of such errors becomes apparent only after extensive testing. One way of circumventing the problem is to use an error margin such that the absolute value of a location difference is compared with a specified error margin rather than with zero. Here the error margin was set at $10^{-15}$ times the tube diameter when geometrical information was used to determine the time of a collision. After collision with a boundary, the position of a particle was reset using the known position of the computational boundary. Because of this repositioning, the system is no longer strictly reversible.

## V. Results and Discussion

### A. Shock Development and Wave Speed

The development of the shock wave is shown in density contour plots, presented in Fig. 2, for all three Mach numbers. Note that the computational conditions that yield these contours provide less accuracy than the conditions used for the final extraction of property profiles but nevertheless display quite well the important features of the shock wave development. One sees a traveling high-density region that constitutes the shock wave. This wave travels downstream with a speed that is seen to be close to the theoretical speed corresponding to an infinitesimally thin shock wave. The reflection of the wave from the end wall is seen clearly; the reflection has not been examined quantitatively.

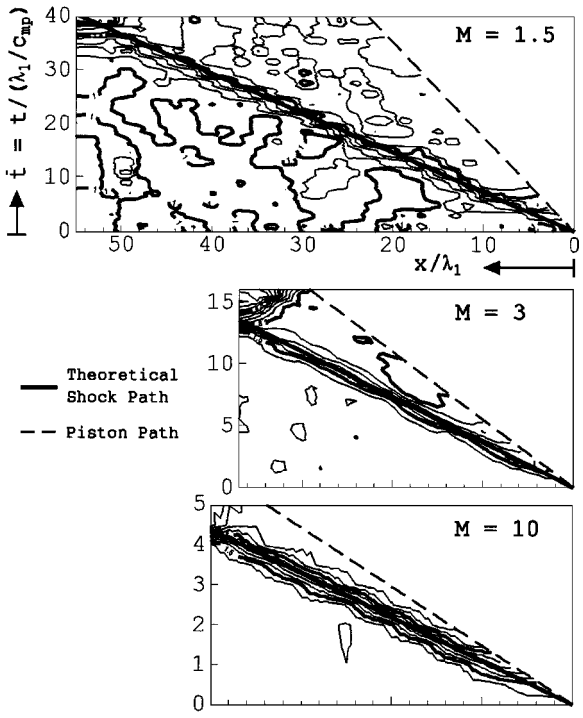


**Fig. 2 Equidensity contour plots.**

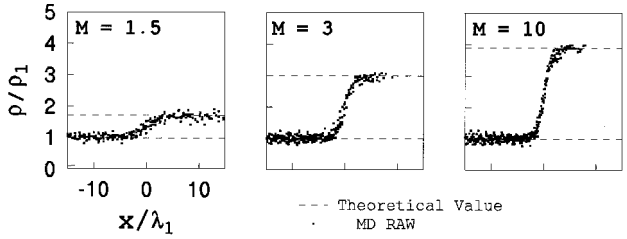


**Fig. 3 Composite profiles of density.**

For the purpose of examining the wave speed and its constancy, composite profiles of the density are shown in Fig. 3. These profiles have shifted the location using the Galilean transformation assuming that the shock speed is the theoretical value but have not further reassigned the location within a cell. For a dynamically ideal system, scatter would be the result of nonconstant shock speed; axial shifting of the profiles, and hence a wide band, would be the result of an incorrect value of the shock speed. It is seen that the band is narrow, the scatter is not large even in the poorest case at Mach 1.5, and the theoretical density ratio is closely achieved. The essential conclusion is that the shock wave is traveling downstream at close to the theoretical wave speed. Numerical values for the scatter are not given here because the final profiles are based on more accurate computations.

### B. Property Profiles

Figure 4 shows density profiles obtained from the composite profiles described in the "Postprocessing of Data" section. The streamwise origin of coordinates is taken as the value corresponding to the midpoint of the density variation. The same origin is later used for the velocity and temperature profiles. The density profiles are monotonic and smooth, the density jumps are within 1.0% of the Rankine–Hugoniot values for Mach 1.5 and 3, and there are indistinguishable differences for Mach 10. For comparison, also shown are profiles obtained by Barnhart (personal communication) using DSMC in a stationary shock computation, following the procedure given by Bird.[27] The Barnhart and Bird profiles appear identical; the recomputation was done to provide accurate numerical values for the comparison, rather than reading results from a published graph.[27] One sees that the MD and DSMC profiles are quite similar, with the MD results having a slightly sharper profile.

**Table 2 Peak values in axial temperature**

| $M$ | MD | DSMC | Yen[29] |
|---|---|---|---|
| 1.5 | 1.51 | 1.50 | 1.51 |
| 3 | 4.24 | 4.13 | 4.27 |
| 10 | 41.40 | 40 | 42.2 |

**Table 3 Shock thickness comparison**

| $M$ | MD | DSMC | Navier–Stokes | Mott-Smith,[12] $u^2$ | Mott-Smith,[12] $u^3$ |
|---|---|---|---|---|---|
| 1.5 | 7.9 | 9.2 | 6.1 | 7.1 | 7.7 |
| 3 | 4.3 | 5.8 | 2.3 | 2.9 | 2.5 |
| 10 | 3.7 | 5.1 | ~1 | 2.2 | 1.7 |

Figure 5 shows the velocity profiles, along with the DSMC results. The DSMC results are shown as continuous curves, although the values are really discrete, so as not to obscure the discrete MD results. The velocity profiles are essentially the inverse of the density profiles, although they were computed separately; the description of the density profiles also applies to the velocity profiles.

The molecular dynamics computations allow collection of energy corresponding to the three perpendicular directions of thermal motion. Thus, one can obtain an axial and two lateral components of temperature. Figure 6 shows the axial component of temperature, along with DSMC results shown as continuous curves. One sees that the axial temperature exhibits a peak within the shock wave. This peak is also found in the DSMC results, the theoretical results of Yen,[28] and experimental results.[29] The MD, DSMC, and Yen's computations give values close to each other; the peak values are given in Table 2. One sees that the spread of peak values is about 3%, a remarkably close agreement inasmuch as the peak values themselves are difficult to obtain in the numerical MD and DSMC computations. Figure 7 shows the lateral components of temperature. The two lateral components are close to each other, as one would expect, and do not display peaks. Figure 8 shows the overall temperature, obtained by adding the energies of the three components. Despite the peak in the axial temperature, the overall temperature behaves monotonically. As with the density and velocity profiles, the MD and DSMC temperature profiles are close to each other, with the MD profile being slightly sharper. Note that the temperature distribution rises upstream of the density distribution in both the MD and DSMC computations.

### C. Shock Thickness

As is traditional, the shock thickness is defined as the distance between intercepts of the maximum slope of the density distribution with the upper and lower values. Normalizing the thickness by the upstream mean free path, the definition becomes

$$\Delta = \frac{n_2 - n_1}{(\mathrm{d}n/\mathrm{d}x)_{\max}} \tag{12}$$

Shock thickness obtained from MD, DSMC, Navier–Stokes, and Mott-Smith[12] computations are plotted in Fig. 9, and numerical values are shown in Table 3. All of the computations show decreasing shock thickness with increasing Mach number. At any given Mach number, the several computations show increasing shock thickness in the following order: Navier–Stokes, Mott-Smith, MD, and DSMC.

### D. Effects of Modifying Computational Region

Several tests were made to examine the effects of decreasing the lateral dimension of the computational region (a smaller tube and, consequently, a larger Knudsen number). Figures 10a–10c show the results of a test at Mach number 1.5, selected because this is an extreme condition for this test. Figure 10a corresponds to the density results already described. Figure 10b is for a higher Knudsen number, unity instead of 0.5. One sees that the scatter is very much greater at the higher Knudsen number. Figure 10c shows the smoothed results for both Knudsen numbers, using the averaging

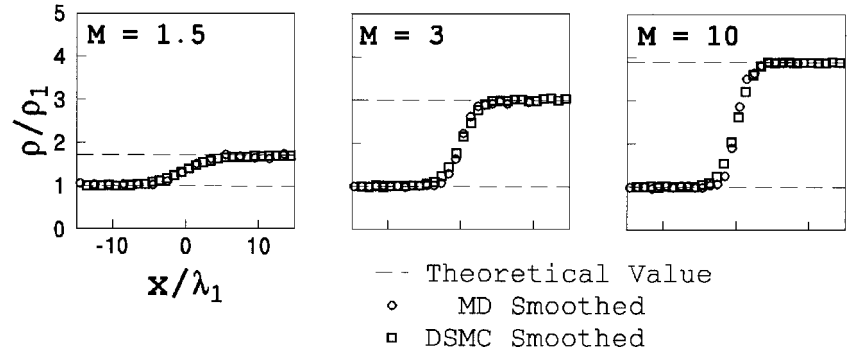


**Fig. 4 Density profiles.**

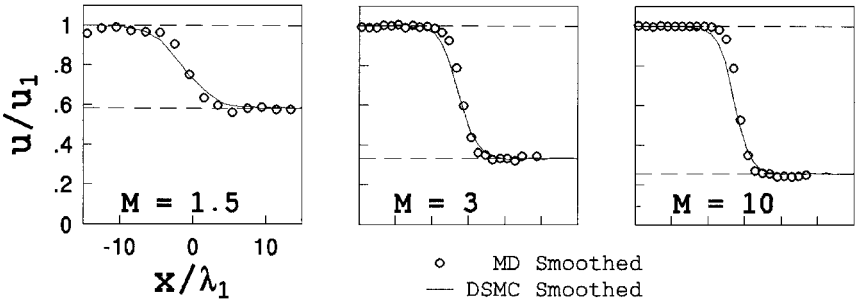


**Fig. 5 Streamwise velocity profiles.**

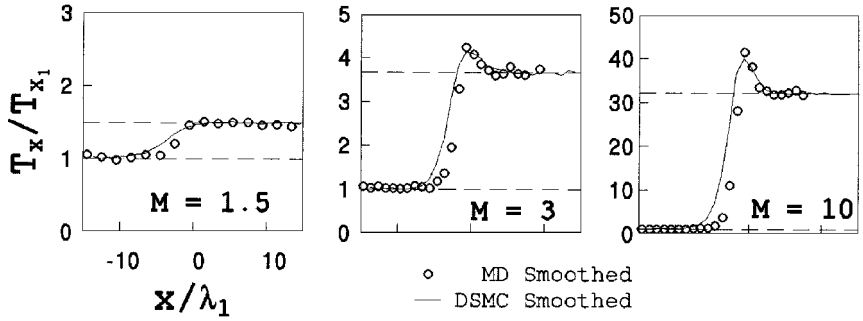


**Fig. 6 Axial temperature profiles.**

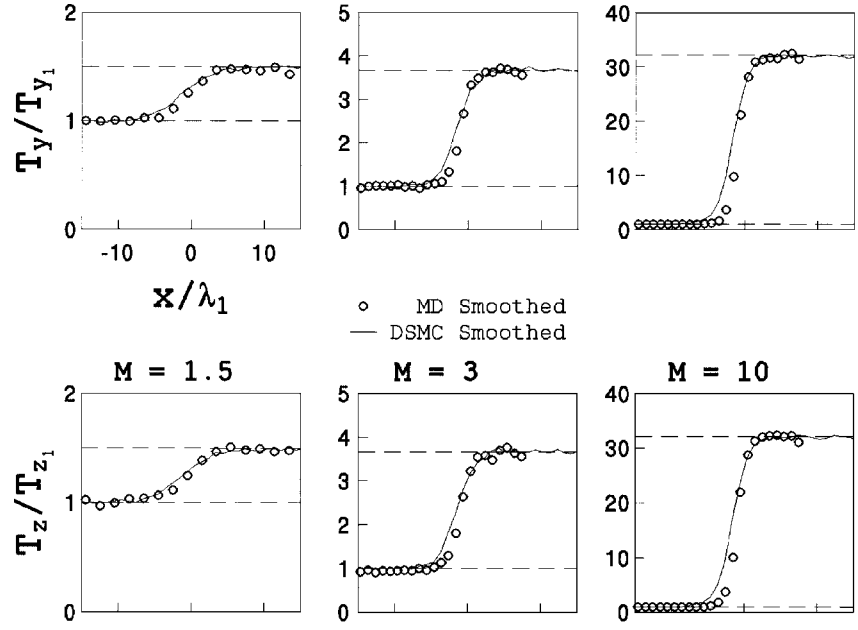


**Fig. 7 Lateral components of temperature.**

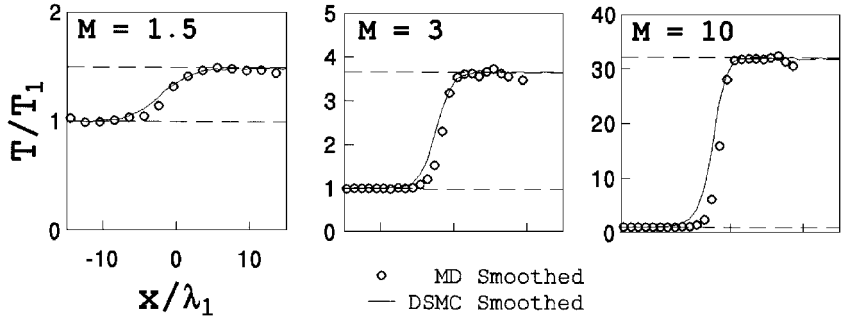


**Fig. 8 Overall temperatures.**

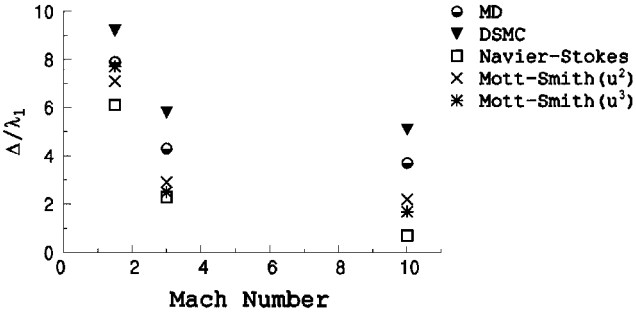


**Fig. 9 Shock thickness comparison.**

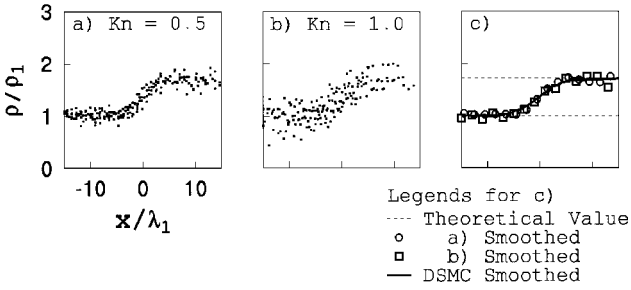


**Fig. 10 Effect of Knudsen number on shock thickness.**

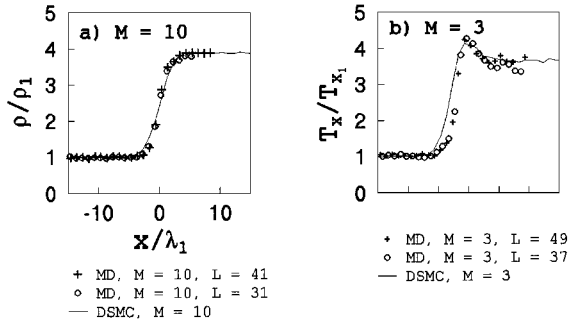


**Fig. 11 Effect of tube length on asymptotic behavior.**

described earlier. One sees that these averaged results are quite close for the two cases, despite the very great scatter in the high-Knudsen-number results.

Tests were also made to examine the effect of tube length on the results. Figure 11a shows density profiles at Mach number 10, and Fig. 11b shows temperature profiles at Mach number 3, each for tubes of different lengths. One sees that the upstream region is essentially the same for the shorter and longer tubes but that the downstream values do not reach the asymptotic limit with the shorter tube. The tube must be long enough to allow full development of the downstream portion of the profiles. This must be examined for each property. At Mach number 10, the critical property was the density, whereas at Mach number 3, it was the temperature. It appears that the appropriate length for full development can be found only by numerical experiment.

## V. Conclusions

The computational results provide an important test of the capabilities of MD in fluid flow applications. We reemphasize that the shock speed, shock profiles, and property jump values are obtained without applying boundary conditions on these values or using any statistical information. The numerical results are close to those obtained using DSMC in a stationary shock formulation, with the MD results displaying slightly sharper shocks. The results also provide a data set from which further questions about the flow behavior can be examined.

## Acknowledgments

This work was supported by a grant from NASA Lewis Research Center, monitored by Dale C. Ferguson. Computer use at NASA Ames Research Center was awarded under the Numerical Aerospace Simulation program. P. Barnhart, Supervisor, Aerospace Analysis Section, NASA Lewis Research Center Group, Sverdrup Technology, Inc., Middleburg Heights, Ohio, is gratefully acknowledged for providing profiles used for comparison purposes.

## References

[1]Rankine, W. J. M., "On the Thermodynamic Theory of Waves of Finite Longitudinal Disturbance," *Transactions of the Royal Society (London)*, Vol. 160, 1870, p. 277.

[2]Lord Rayleigh, J., "Aerial Plane Waves of Finite Amplitude," *Proceedings of the Royal Society of London*, Vol. A84, 1910, p. 247.

[3]Taylor, G. I., "The Conditions Necessary for Discontinuous Motion in Gases," *Proceedings of the Royal Society of London*, Vol. A84, 1910, p. 371.

[4]Becker, R., "Stoßwelle und detonation," *Zeitschrift für Physik*, Vol. 8, 1921–1922, pp. 321–362.

[5]Thomas, L. H., "Note on the Becker's Theory of the Shock Front," *Journal of Chemical Physics*, Vol. 12, No. 11, 1944, p. 449.

[6]Gilbarg, D., "The Existence and Limiting Behavior of the One-Dimensional Shock Layer," *American Journal of Mathematics*, Vol. 73, No. 2, 1951, pp. 256–274.

[7]Von Mises, R., "On the Thickness of a Steady Shock Wave," *Journal of the Aeronautical Sciences*, Vol. 18, 1950, pp. 551–554.

[8]Zoller, K., "Zur Struktur des Verdichtungsstoßes," *Zeitschrift für Physik*, Vol. 130, 1951, pp. 1–38.

[9]Chapman, S., and Cowling, T. G., *The Mathematical Theory of Non-uniform Gases*, Cambridge Univ. Press, Cambridge, England, UK, 1939.

[10]Grad, H., "On the Kinetic Theory of Rarefied Gases," *Communications on Pure and Applied Mathematics*, Vol. 2, No. 4, 1949, pp. 331–407.

[11]Grad, H., "The Profiles of a Steady Plane Shock Wave," *Communications on Pure and Applied Mathematics*, Vol. 5, 1952, pp. 257–300.

[12]Mott-Smith, H. M., "The Solution of the Boltzmann Equation for a Shock Wave," *Physical Review*, Vol. 82, No. 6, 1951, p. 885.

[13]Gilbarg, D., and Paolucci, D., "The Structure of Shock Waves in the Continuum Theory of Fluids," *Journal of Rational Mechanics and Analysis*, Vol. 2, 1953, p. 617.

[14]Radin, S. H., and Mintzer, D., "Orthogonal Polynomial Solution of the Boltzmann Equation for a Strong Shock," *Physics of Fluids*, Vol. 9, No. 9, 1966, p. 1621.

[15]Rode, D. L., and Tanenbaum, B. S., "Mott-Smith Shock Thickness Calculations Using the $v_x^p$ Method," *Physics of Fluids*, Vol. 10, 1967, p. 1352.

[16]Bird, G. A., "Approach to Transitional Equilibrium in a Rigid Sphere Gas," *Physics of Fluids*, Vol. 6, 1963, p. 1518.

[17]Bird, G. A., "Shock-Wave Structure in a Rigid Sphere Gas," *Rarefied Gas Dynamics*, edited by de Leeuw, Academic, New York, 1965, p. 216.

[18]Tsai, D. H., and Trevino, S. F., "Thermal Relaxation in a Dense Liquid Under Shock Compression," *Physical Review A*, Vol. 24, No. 5, 1981, p. 2743.

[19]Hoover, W. G., "Structure of Shock-Wave Front in a Liquid," *Physical Review Letters*, Vol. 42, No. 23, 1979, p. 1531.

[20]Niki, K., and Ono, S., "Molecular Dynamics Study on the Structure of Shock Wave Front in a Hard-Core Fluid," *Physics Letters*, Vol. 62A, No. 6, 1977, p. 427.

[21]Bird, G. A., *Molecular Gas Dynamics and the Direct Simulation of Gas Flows*, Oxford Univ. Press, New York, 1994, pp. 316–333.

[22]Woo, M., "Molecular Dynamics Simulation of a Piston Driven Shock Wave in a Hard Sphere Gas," Ph.D. Dissertation, Dept. of Mechanical and Aerospace Engineering, Case Western Reserve Univ., Cleveland, OH, May 1994.

[23]Woo, M., and Greber, I., "Molecular Dynamics Simulation of a Piston Driven Shock Wave in a Hard Sphere Gas," *APS Bulletin*, Vol. 39, No. 9, 1994, p. 1908.

[24]Horowitz, J., Woo, M., and Greber, I., "Molecular Dynamics Simulation of a Piston-Driven Shock Wave," *Physics of Fluids*, Vol. 7, No. 9, 1995, p. S6.

[25]Greber, I., and Wachman, H., "Scaling Rules and Time Averaging in Molecular Dynamics Computations of Transport Properties," *Rarefied Gas Dynamics: Theoretical and Computational Techniques*, edited by E. P. Muntz, D. P. Weaver, and D. H. Campbell, Vol. 118, Progress in Astronautics and Aeronautics, AIAA, Washington, DC, 1989, pp. 194–207.

[26]"Coplot Manual Revision 2.02," Cohort Software, Berkeley, CA, 1990, p. 88.

[27]Bird, G. A., "Velocity Distribution Function Within a Shock Wave," *Journal of Fluid Mechanics*, Vol. 30, Pt. 3, 1967, p. 479.

[28]Yen, S.-M., "Temperature Overshoot in Shock Waves," *Physics of Fluids*, Vol. 9, No. 7, 1966, p. 1417.

[29]Muntz, E. P., and Harnett, L. N., "Molecular Velocity Distribution Function Measurements in a Normal Shock Wave," *Physics of Fluids*, Vol. 12, No. 10, 1969, p. 2027.

K. Kailasanath
*Associate Editor*